Pergamon

Int. J. Impact Engng. Vol. 17, pp. 387–398, 1995

0734-743X/95 $9.50+0.00

VERIFICATION OF THE EQUATION FOR RADIAL CRATER GROWTH BY SHAPED CHARGE JET PENETRATION

Manfred Held
Deutsche Aerospace AG
86523 Schrobenhausen, Germany

Summary-The radial crater growing process, caused by a shaped charge jet penetrating into water, has been measured for the first time with high space and time resolution, using the socalled profile streak technique. The results confirm very well the analytical model of the crater radius as a function of time, which was for the first time presented by Szendrei and which has been slightly modified by the author.

INTRODUCTION

The axial penetration of shaped charge jets has been described a long time ago. A good overview of various older Ballistic Research Laboratory (BRL) reports which are based on the hydrodynamic or Bernoulli law can be found in 1. Detailed derivations of the behavior of penetrating jets, either continuous, fully particulated, or a mixture of the two, have been recently summarized by the author 2. The axial cratering process as measured in water can be relatively well predicted by these simple equations 3. But the physics can be improved, if for the axial penetration, compressibility and afterflow effects are taken into account 4.

Szendrei 5. has presented an analytical equation for the radial growth of the crater as a function of jet velocity, jet diameter at the crater bottom, and the target strength. Held 6. has already used this equation to calculate the penetration capability of shaped charges whose axes are inclined to the flight direction which depends strongly on the crater radius. This is the only equation at present known to the author for the purpose of determining crater radius as a function of time.

RADIAL CRATER GROWTH THEORY

Due to a slight modification introduced into the basic equations of the Szendrei theory 5. the derivation is given in detail below. With the modified Bernoulli equation the stagnation pressure p is related to the axial cratering velocity u and to the material strength R_t

$$p = 1/2 \cdot \varrho_t \cdot u^2 + R_t \qquad (1)$$

Szendrei 5. has set the radial crater growth velocity u_C equal to the forward or axial cratering velocity u:

$$u_C = u \tag{2}$$

Thus, the radial cratering velocity u_C can be obtained by rearranging equation (1):

$$u_C = \left(\frac{2p}{\varrho_t} - \frac{2R_t}{\varrho_t}\right)^{1/2} \tag{3}$$

The pressure p changes as the radius increases. Therefore, Szendrei 5. used the plausible assumption that the force would always remain constant, i.e., that pressure times area $(p \cdot a)$ is a constant, whence

$$p = p_0 \cdot (a_0/a) \tag{4}$$

where p_0 is the stagnation pressure and a_0 is the area of the jet at the crater bottom.

For the initial stagnation pressure p_0 of a penetrating jet with its high velocities, the target strength R_t can be neglected. R_t is generally smaller than p_0 by more than two orders of magnitude. Therefore the simple Bernoulli equation can be used, for which the initial stagnation pressure p_0 is equal to half the density of the jet ϱ_j times the square of the difference of jet to cratering velocity $(v_j - u)$:

$$p_0 = 1/2 \cdot \varrho_j \cdot (v_j - u)^2 \tag{5}$$

The cratering velocity u is a function of jet velocity v_j and square root of the ratio of target to jet density:

$$u = v_j/(1 + \sqrt{\varrho_t/\varrho_j}) \tag{6}$$

Equation (6) in equation (5) gives:

$$p_0 = \frac{\varrho_t \cdot v_j^2}{2 \cdot (1 + \sqrt{\varrho_t/\varrho_j})^2} \tag{7}$$

For a_0/a we can write r_j^2/r_C^2, the square of the jet- to crater-radius ratio, and using equations (4) and (5) to substitute p and p_0, respectively, we can re-write equation (3) in the form:

$$\frac{dr_C}{dt} = \left(\frac{r_j^2 \cdot v_j^2}{r_C^2 (1 + \sqrt{\varrho_t/\varrho_j})^2} - \frac{2 \cdot R_t}{\varrho_t}\right)^{1/2} \tag{8}$$

This equation (8) can be separated with respect to the variables, time t and radius r_C, and can be re-written in the following form:

$$dt = \frac{dr_C}{\left(\frac{2 \cdot r_j^2 \cdot p_0}{r_C^2 \cdot \varrho_t} - \frac{2R_t}{\varrho_t}\right)^{1/2}} \tag{9}$$

This expression can be simplified:

$$dt = \frac{dr_C}{\sqrt{A/r_C^2 - B}} \tag{10}$$

with

$$A = \frac{2 \cdot r_j^2 \cdot p_0}{\varrho_t} = \frac{r_j^2 \cdot v_j^2}{(1 + \varrho_t/\varrho_j)^2} = r_j^2 \cdot u^2 \tag{11}$$

and

$$B = 2\, R_t/\varrho_t \tag{12}$$

The integration of equation (10) gives the time t for the growth of the crater r_C:

$$t = \frac{1}{\sqrt{B}} \left(\sqrt{A/B - r_j^2} - \sqrt{A/B - r_C^2} \right) \qquad (13)$$

This equation can now be analysed. For example the crater will no longer grow, when

$$r^2_{c,m} = A/B \qquad \text{or} \qquad r_{c,m} = \sqrt{A/B} \qquad (14)$$

$r_{c,m}$ is the maximum achievable crater radius.

The final time t_f for the radial cratering process is given with

$$t_f = \frac{\sqrt{A/B - r_j^2}}{\sqrt{B}} \qquad (15)$$

Equation (13) can also be solved for the crater radius r_C as a function of time t:

$$r_C = \sqrt{A/B - \left(\sqrt{A/B - r_j^2} - t\sqrt{B}\right)^2} \qquad (16)$$

The crater radius r_C can be calculated as a function of time by applying equation (16) which, again, requires the following data:

jet radius r_j
jet velocity v_j
jet density ϱ_j
target density ϱ_t
target resistance R_t

The density is known, and the jet velocity at the crater bottom can be easily calculated. However the jet radius r_j is somewhat uncertain.

CRATER GROWTH PREDICTION

For the shaped charge and barrier thicknesses chosen, the in Table 1 listed jet characteristics are given at the streak observation plane. For the calculation of "A" equation (11) was used. For the target strengh R_t it is simple used the hydrostatic pressure of the water head. For the water depth of 0.15 m, corresponding to a pressure of $1{,}5 \cdot 10^3$ N/m^2 or $1{,}5 \cdot 10^3$ Pa, the value for constant B is given by the equation (12):

$$B = 2R_t/\varrho_t = 2 \cdot 1{,}5 \cdot 10^3 \frac{\text{kg} \cdot \text{m/sec}^2}{\text{m}^2} / 10^3 \frac{\text{kg}}{\text{m}^3} = 3 \text{ m}^2/\text{sec}^2 \qquad (12n)$$

Table 1 Jet velocities v_j, corresponding axial cratering velocities u and jet radius r_{jC} at the observation plane (see Appendixes A and B).

v_j (mm/us)	6.2	6.0	5.0	4.0	3.1
u (mm/us)	4.6	4.5	3.7	3.0	2.3
r_{jC} (mm)	0.81	0.82	0.96	1.15	1.50
A (m^4/s^2)	13.9	13.6	12.6	11.9	11.9
B (m^2/s^2)	3	3	3	3	3

With these data of Table 1 the crater radius r_C can be calculated as a function of time t by equation (16). As an example the crater radii for the most extreme conditions of Table 1, first with v_j = 6.2 mm/us and r_{jC} = 0.81 mm, and then with v_j = 3.1 mm/us and r_{jC} = 1.5 mm, using respectively the constants 13.9 m^4/sec^2 and 11.9 m^4/sec^2 are presented in Table 2.

Table 2 Calculated radial crater r_C as a function of time for the two extremes after Table 1.

t (us)	05	10	15	20	30	40	50	60	70	80
r_C (mm) (6.2mm/us)	6.1	8.7	10.6	12.3	15.0	17.3	19.4	21.2	22.9	24.5
r_C (mm) (3.1mm/us)	6.0	8.3	10.2	11.7	14.3	16.5	18.4	20.2	21.8	23.3

Surprisingly the radii during the crater growth process lie closely together. The reason for this is that the parameter "A" is very similar throughout; the products $v_j \cdot r_{Cj}$ are nearly constant. With decreasing velocity the jet diameter increases correspondingly.

EXPERIMENTAL VERIFICATION

The initial phase of crater growth process can be very well observed in water (7. and 8.). This technique was used to check the radial growth process as a function of different jet, and hence cratering velocities. For this purpose a test set-up was used with a barrier of variable thickness x in front of a water tank. Fig. 1 shows the test set up with the shaped charge used (KB 44, which has 44 mm outside diameter, 42 mm liner diameter, 1 mm thick, in copper, of 60° included angle). With a wave shaper the jet tip velocity v_{j0} is 8.3 mm/us. The standoff was constant at 88 mm (two calibers) to the front surface of the barrier, which is 108 mm from the virtual origin, Z_0. The barrier, of mild steel, was in contact with the 5 mm plexiglass side wall of the water tank. The water tank was cubic with dimensions of 300 mm and consisted of 5 mm plexiglass plates. The jet was aimed at the middle of the water tank and perpendicular to the observation plane (streak plane). The reason for this was to get the maximum observation time before shock waves reach the side walls and make the observation impossible by the formation of cavitation bubbles by the rarefaction fan.

The water tank and therefore the crater formation was front-illuminated by two Argon bombs. Their axes were about 30° to the axis of the camera lens. Green paper - not shown in the figure -was placed behind the water tank to get some back-illumination for shadowgraphs of the crater formation (Fig. 2).

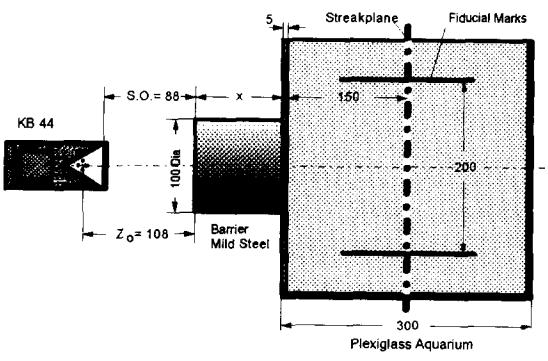

Fig. 1 Test Set-up

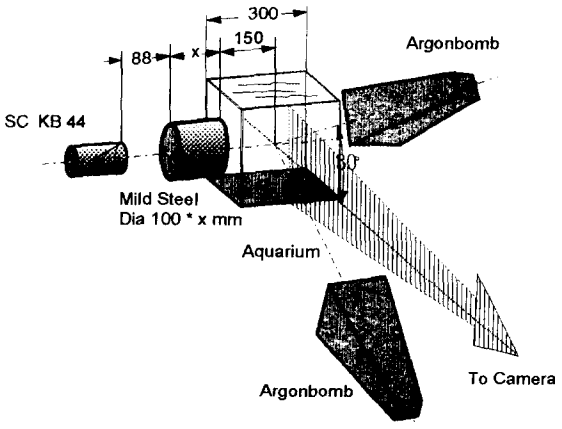

Fig. 2 Front illumination

The events were recorded by the continuously writing simultaneous streak and framing camera CORDIN Model 330 9. The writing speed for the streak record was about 0.75 mm/us and the framing rate was around 135,000 frames/sec. Streak and framing records were generally made on Fujicolor ASA 1600. The test set-up was arranged at about 3.5 m from the 600 mm focal

Table 3 Summary of Experimental Data

v_j (mm/μs)	SC. No.	Barrier (mm)	Frames Fr/sec	Frames Δt (μs)	v_{Streak} (mm/μs)	t_A Theor. (μs)	t_A meas. (μs)	Film Typ	Pen. (C15) (mm)
6.2	50562	0	131296	7.616	0.71	41.6	43.8	Fujicolor ASA 1600	130/135
6.0	50634	5	139380	7.175	0.72	43.8	48.4	Kodak ASA 1000	--
5.0	50563	36	135922	7.353	0.74	58.8	60.1	Fujicolor ASA 1600	103
4.0	50564	83	133067	7.515	0.72	85.2	87.4	Fujicolor ASA 1600	Slug
3.1	50565	143	134338	7.442	0.73	127.3	129.1	Fujicolor ASA 1600	35

The framing pictures obtained for jet velocities of v_j = 6 mm/us, v_j = 4 mm/us and v_j = 3 mm/us are shown in Figs. 3, 4 and 5.

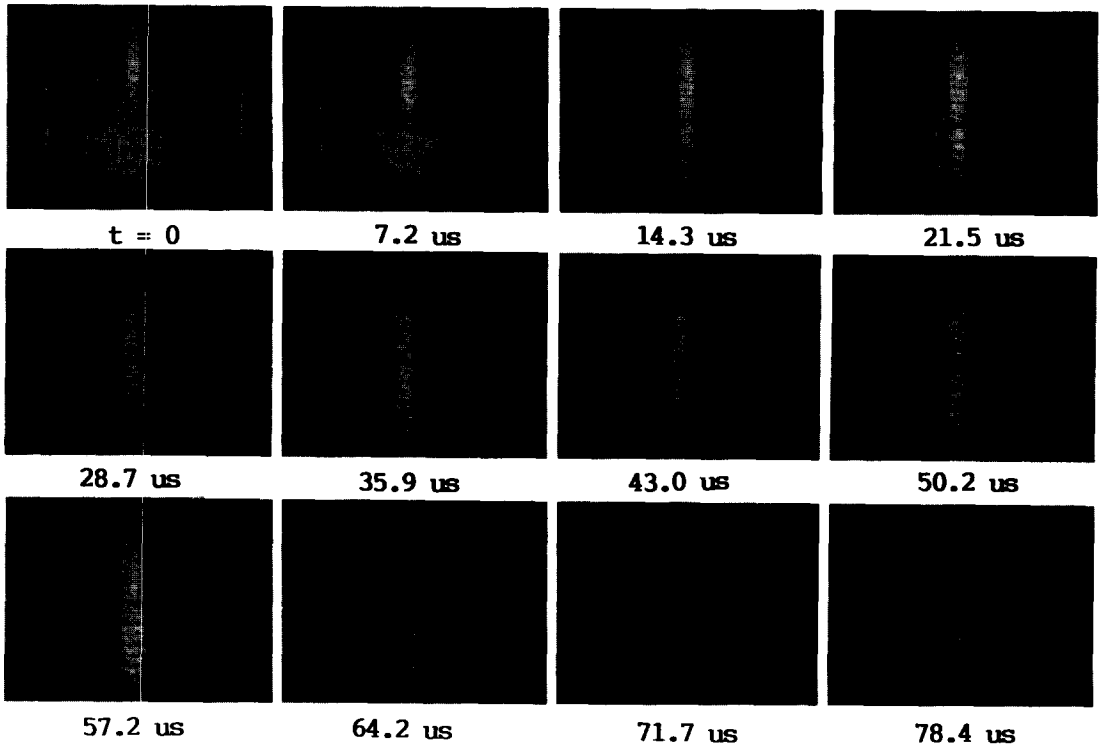

Fig.3 v_j = 6 mm/us at the streak plane (SC 50634)

The continuously penetrating jet at 6 mm/us (Fig. 3) arrives after 43.8 us at the streak slit (black line on the figures). The arrival time of the jet on the streak plane is used as the time t_0 for the analysis of the frames and streak records. At early times the crater has a relatively smooth surface, which later looks rougher, lower down on the individual pictures. The more undulating crater arises from the fact that the jet is necked after its longer penetration time through the water target. The appearance of rarefaction fans creates cavitation bubbles impairing the transparency of the water after about 80 us.

The undulating structure of the crater is more pronounced in the frames with the jet velocity of 4 mm/us and an arrival time of 87 us (Fig. 4). In this case we have a fully particulated jet. The "bubble" lengths can be very well correlated with the lengths of the discrete particles.

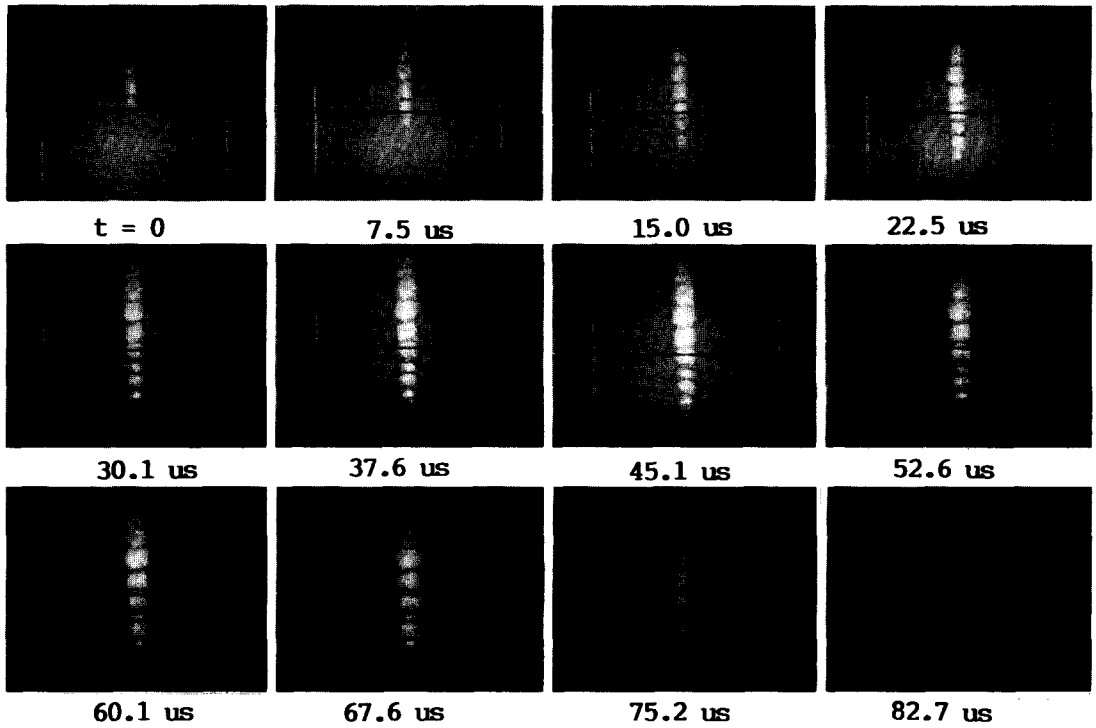

Fig.4 v_j = 4 mm/us at the streak plane (SC 50564)

On the fourth frame of Fig. 4 we can see the streak slit just in the middle of the bubble, on the 12th frame it is very near to the next necking point. This means that the bubble is moving with the relatively low velocity of about 0.2 mm/us in the direction of the jet. This needs to be taken into account when analysing streak records of the crater growth process. The "same" plane of the radial crater growth process is not being observed in each case.

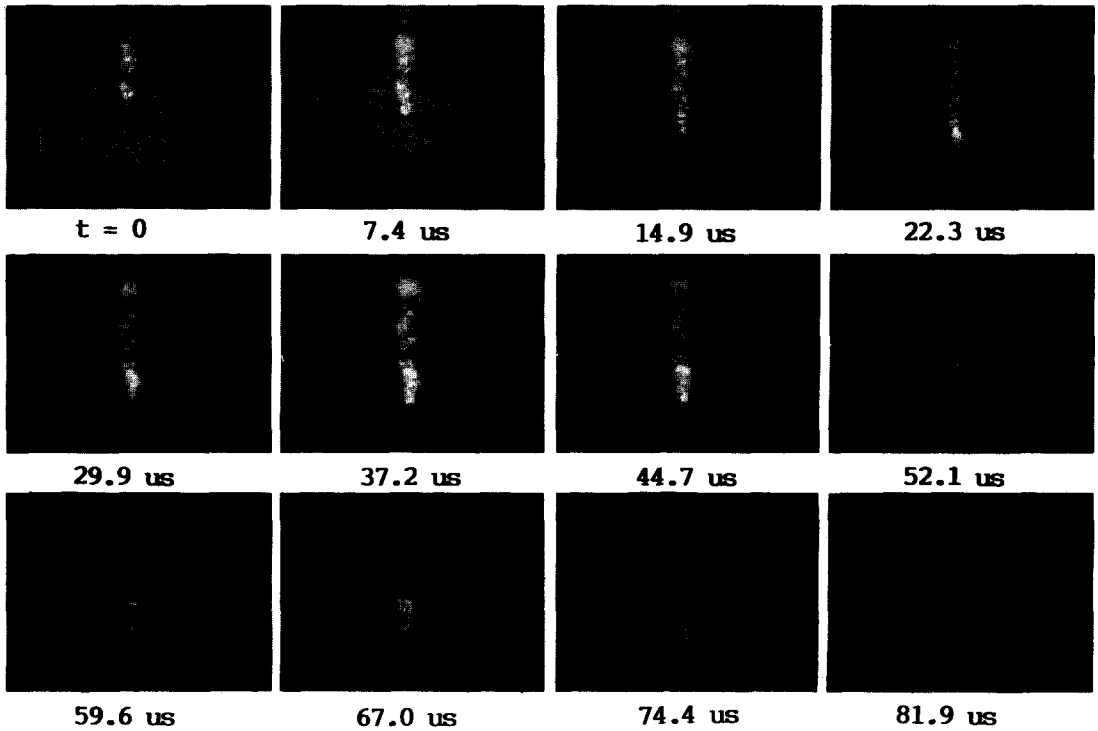

Fig.5 v_j=3 mm/us at the streak plane (SC 50565)

If we look now at the frames of a jet which has been particulated for some time (127 us - 82 us = 45 us), we observe a very irregular structure of the crater wall (Fig. 5). This phenomenon arises from poorly aligned and tumbling particles.

A comparison of the crater formation under the different jet conditions - continuous, necked, or particulated - along with their different velocities, is given in Fig. 6, observing at the middle of the water tank at times after arrival of zero, 22,5 us, and 45 us.

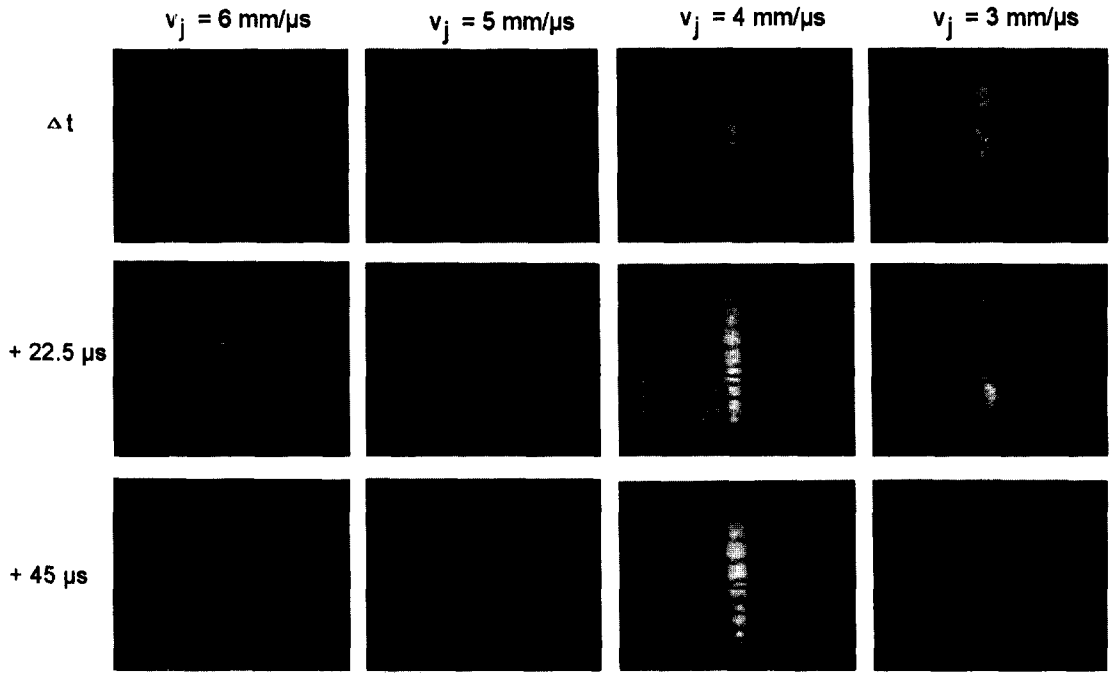

Fig.6 Comparison of the frames, obtained at different jet velocities

The gained streak records simultaneously with the frames are not reproduced here; their contrast in black and white would be too low. But the coloured streak records were enlarged by a factor of about five, and the shock waves and crater profiles have been processed as a function of time using a digitizer table. These values have been printed out and are shown in Fig. 7 in an enlarged version. The results from the four further experiments are presented in Fig. 8.

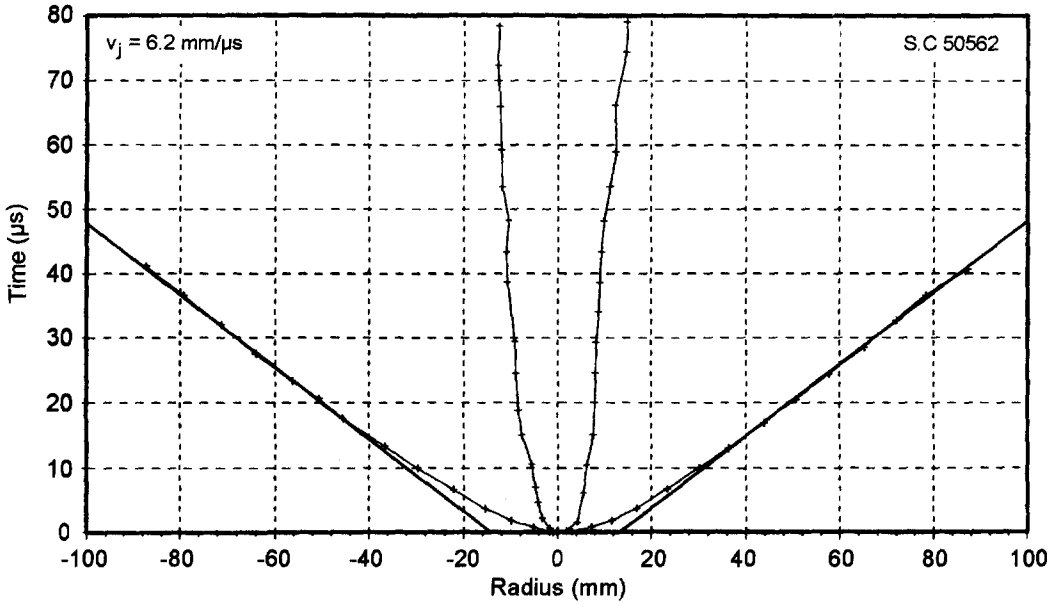

Fig. 7 Shock velocity and crater growth for v_j = 6.2 mm/us

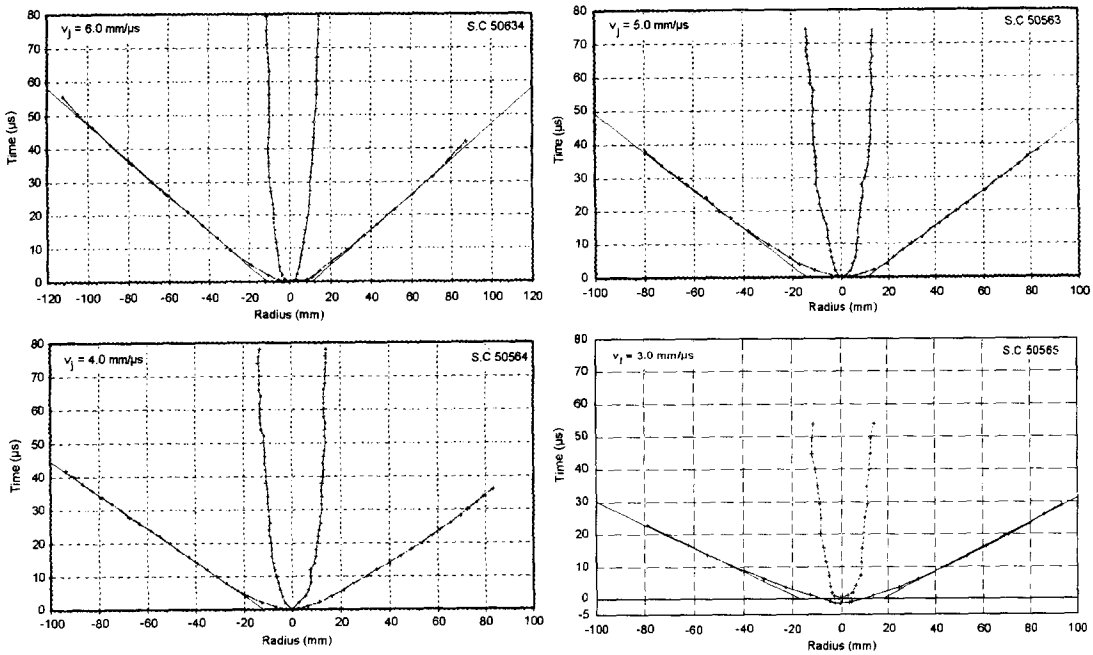

Fig. 8 Analysis of shock velocities and crater growth processes at different jet velocities.

The curves of crater radius as a function of time all look very similar, even though there was more than a factor of two in jet velocity, and hence axial in cratering velocity. The observation time is in the range of 80 us, that is, before the rarefaction fan from cavitation destroys the transparency of the water.

ANALYSIS

The results obtained experimentally for the radial crater growth at different jet velocities are summarized in Fig. 9.

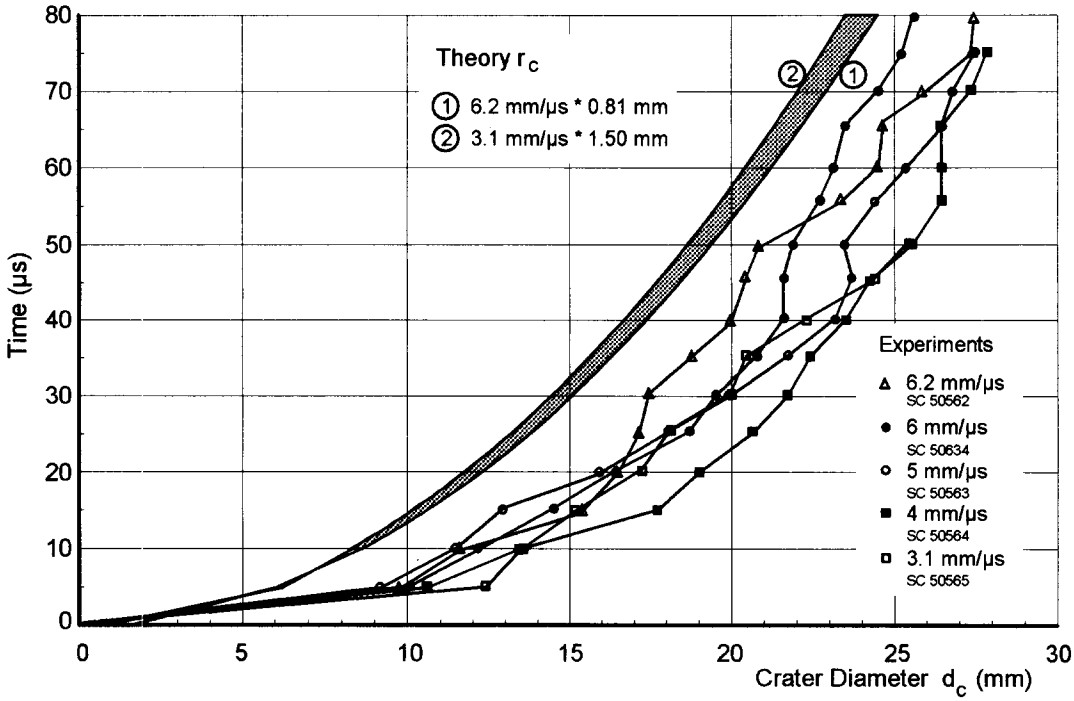

Fig. 9 Crater growth as a function of time from experiment and according to theory

The theoretical predictions are given for a jet velocity of 6.2 mm/us and 0.81 mm jet radius, and for 3.1 mm/us velocity and 1.5 mm radius (see Table 2).

The values obtained experimentally lie very close together, as predicted by the theory. As mentioned before, the product of jet velocity, or rather, of axial crater propagation velocity, and jet radius remained nearly constant in these tests. According to the theory presented here, this parameter determines the crater radius. The shape of the experimental curve also agrees well with the slope of the theoretical prediction.

However, in the diagram (Fig. 9) the values from the experiments are given as crater diameter, but from the theory in radius. This means that experiment gives smaller diameters by a factor of nearly two compared with theory. This may arise for several different reasons:

i.) The "effective" jet diameter may be smaller than that measured, because of the formation of a hemispherical nose 10.

ii.) The penetrating jet may form a "Kernel" after Backofen's ideas 11., which implies a reduced effective jet diameter.

iii.) The dynamic strength of water may be much higher than that implied by taking simply the static pressure (to match the experimental crater diameters at 80 us, the strength would have to be 20,000 times higher, which seems unlikely).

iv.) A combination of all of these effects: both higher target strength with viscoplastic behaviour, and also smaller effective jet diameters.

Since there is less than a factor of two between the radii predicted by the relatively simple crater growth theory and those obtained experimentally, it can be concluded that the principal assumptions and the physical basis of the suggested theory are valid.

REFERENCES

1. W.P. Walters and J.A. Zukas, "Fundamentals of Shaped Charges" Pages 137-142, John Wiley & Sons, 1989
2. M. Held, "Hydrodynamic Theory of Shaped Charge Jet Penetration", Journal of Explosives and Propellants, R.O.C. Taiwan, 7, 9-24, 1991
3. M. Held and J. Backofen, "Penetration of Shaped Charge Jets into Water", Proceedings of 12th Int. Symposium on Ballistics Vol II, 30-40, 1990
4. J. Backofen, "Supersonic Compressible Penetration Modeling for Shaped Charge Jets", Proceedings of 11th Int. Symposium on Ballistics, 395-406, 1989
5. T. Szendrei, "Analytical Model of Crater Formation by Jet Impact and its Application to Calculation of Penetration Curves and Hole Profiles", Proceedings of 7th Int. Symposium on Ballistics, 575-583, 1983
6. M. Held, "Transverse Shaped Charges", Proceedings of 8th Int. Symposium on Ballistics, VII: 39-47, 1984
7. M. Held, D. Jiang, C.C. Chang and N.S. Huang, "Crater Growing Process of Water by Shaped Charge Penetration", 21. Int. Congress on High Speed Photography and Photonics, 1994
8. M. Held, N.S. Huang, D. Jiang and C.C. Chang, "Determination of the Crater Radius as a Function of Time of a Shaped Charge Jet that Penetrates Water", Propellant, Explosives, Pyrotechnics: Submitted
9. Company Cordin, 2230 South, 3270 West, Salt Like City, Utah, 84119, USA
10. H.R. James, "Critical Energy Criterion for Shock Initiation of Explosives by Projectile Impact", Propellants, Explosives, Pyrotechnics 13, 35-41, 1988
11. J. Backofen, "A Post-Perforation Kernel Acceleration Model", Proceedings of 14th Int. Symposium on Ballistics, Vol. 2, 639-649, 1993

APPENDIX A

CALCULATION OF CRATER BOTTOM VELOCITY

The equations applied for the calculation of shaped charge jet penetration into a target are derived and explained in detail in <2>. The jet velocity v_j of a continuously stretching jet after passing through a target of thickness P can be calculated using equation (22) according to Ref. <2>:

$$v_j = v_{j0} \cdot (Z_0/(P + Z_0))^{\gamma} \qquad (1A)$$

where v_{j0} is the jet tip velocity, Z_0 the distance from the virtual origin to the target surface and γ is the square root of target (water) to jet (copper) density ratio ($\gamma = \sqrt{\varrho_t/\varrho_j}$).

In this case the crater bottom velocity u is a simple function of the jet velocity according to equation (4) of <2> or to equation (6):

$$u = v_j/(1 + \gamma) \qquad (2A)$$

Taking the values for a copper jet penetrating into water,

$$u = 0{,}75 \cdot v_j \qquad (2An)$$

The residual jet velocity v_j, - penetration occurs first by a continuously stretching jet and then by a particulated jet - is a function of the crater depth P, the distance Z_0 from the virtual origin to the water surface, the square root from the ratio of the target density to the jet density, γ, the particulation time t_p and a constant E ((50.2) of <2>)

$$v_j = (E - (P + Z_0) \cdot \gamma)/t_p \qquad (3A)$$

A particulated jet gives a series of discrete movements of the axial crater. The cratering velocity for each discrete particle is given by equation (2A). However the mean crater bottom velocity u is given in this case by equation (60) of <2>:

$$u = v_j^2 \cdot t_p/E \qquad (4A)$$

The constant E is determined by equation 49 in <2>:

$$E = (\gamma + 1) \cdot v_{j0} \cdot t_0^{\gamma/(1+\gamma)} \cdot t_p^{1/(1+\gamma)} \qquad (5A)$$

The numerical calculations for the axial cratering velocities are given below. The jet characteristics for these experiments are

v_{j0} = 8.3 mm/us
Z_0 = 108 mm
t_{P1} = 64 us (for v_j = 8.3 mm/us - 5.5 mm/us)
t_{P2} = 82 us (for v_j = 5.5 mm/us - 3.0 mm/us)

With no barrier, equation (1A) has to be used in its original form for the penetration of water:

$v_{j0} = 8.3 \cdot (108/(150+108))^{0.335} = 6.2$ mm/us

The arrival time t_A is the distance divided by the jet velocity, which is just arriving on the crater bottom. It can be assumed that the jet veocity is constant over the short distance.

$t_A = d/v_j = (150+108)/6.2 = 41.6$ us

41.6 us is less than the first particulation time t_{P1} of 64 us for this jet. This means the jet is penetrating continuously, in an unbroken state.

For a composite target having two densities, equation (1A) has to be modified appropriately. First one must calculate the residual jet velocity behind the 5 mm steel barrier (density 7.85 g/cm^3).

$v_{jR} = 8.3 \cdot (108/(5+108))^{0.939} = 7.955$ mm/us

With this residual jet velocity v_{jR} and the now greater distance Z_0 from the virtual origin, the jet velocity after 150 mm penetration of the water layer (density 1 g/cm^3), can be calculated.

$v_j = 7.955((108+5)/(150+108+5))^{0.335} = 6.0$ mm/us
$t_A = (108+5+150)/6.0 = 43.8$ us

The arrival time t_A is still much less than the particulation time. Using the same procedure the values for steel barriers of thickness 36 mm and 83 mm one can calculate:

36 mm barrier thickness

$v_{jR} = 8.3 \cdot (108/(36+108)^{0.939} = 6.335$ mm/us
$v_j = 6.335 \cdot ((108+36)/(150+108+36))^{0.335} = 5.0$ mm/us
$t_A = (108+36+150)/5.0 = 58.8$ us

83 mm barrier thickness

$v_{jR} = 8.3 \cdot (108/(883+108))^{0.939} = 4.85$ mm/us

$v_j = 4.859((108+83)/(150+108+83))^{0.335} = 4.0$ mm/us

$t_A = (150+108+83)/4.0 = 85.2$ us

The arrival time t_A with the jet of 4 mm/us is just above the particulation time of 82 us. This means that the calculation is still basically correct, but the record from the framing camera shows that penetration has taken place entirely by discrete particles.

143 mm barrier thickness

$v_{jR} = 8.3 \cdot (108/(143+108))^{0.939} = 3.759$ mm/us

$t_A = (108+143)/3.759 = 66.8$ us

The part of the jet with the velocity of 3.8 mm/us is not particulated, when it starts to penetrate the water layer. Although at first continuously penetrating, the jet will later go on to penetrate in particulated form. For this reason equations (5A) and (3A) must be used:

$B = 1.335 \cdot 3.759 \cdot 66.8^{0.251} \cdot 82^{0.75} = 392.6$ mm

$v_j = (392.6 - (150+108+143) \cdot 0.335)/82 = 3.15$ mm/us

$t_A = (108+143+150)/3.15 = 127.3$ us

The cratering velocity for the "discrete" particle with velocity 3.15 mm/us is given by equation (2A):

$u = 3.15/(1+0.335) = 2.36$ mm/us

The "mean cratering" velocity is given by equation (4A):

$u = 3.15^2 \cdot 82/392.6 = 2.07$ mm/us

For the radial crater expansion process, the value appropriate to cratering by a discrete particle at a velocity of 2.36 mm/us has to be taken.
All derived jet and cratering values are summarized in Table 1.

APPENDIX B

The jet radii in Table 1 are derived from the measured diameters from a flash-X-ray picture of a particulated jet. From these, the diameters were calculated at the arrival times t_A of the jets at the observation plane. Taking into account the particulation times t_{Pn} and using the following equation, one obtains these values by conserving mass. The values used are summarized in Table B.

$$r_{jC} = 0.5 \cdot d_j \cdot \sqrt{t_{Pn}/t_A} \qquad (1B)$$

Table B Calculation of jet radii r_{jC} at the observation plane for the different tests

v_j (mm/us)	6.2	6.0	5.0	4.0	3.0
d_j (mm)	1.30	1.35	1.65	2.30	3.00
t_P (us)	64	64	82	82	82
t_A (us)	41.6	43.8	58.8	85.2	127.3
t_P/t_A	1.24	1.21	1.18	1	1
r_{jC} (mm)	0.81	0.82	0.96	1.15	1.50